

Dyke-maintained rift segmentation at continental rupture – the 2005 Dabbahu (Afar) rifting episode

Tim Wright, C. Ebinger, J. Biggs, A. Ayele, G. Yirgu, D. Keir, and A. Stork

Supplementary Information

Structure of the Dabbahu Magmatic Segment

The Dabbahu and adjacent magmatic segments formed between ~4 and 2 Ma (Barberi and Varet, 1977; Hayward and Ebinger, 1996) (Fig. SM1). From stereographic analyses of 1:100000 scale imagery, fault density is highest in the axial zone, where faults have a mean length of 2.5 km (Hayward and Ebinger, 1996). Many of the central graben faults have small volume fissural flows along their length, or cut small eruptive centres (Fig. SM3). Although of lower relief, Quaternary stratovolcanoes dissected by normal faults mark the central portion of the Dabbahu segment, attesting to Quaternary magma sources at the centre of the segment (Fig. SM1). Fault patterns on the rift flanks show the same along-axis segmentation, indicating the locations of magma source(s) have been stable for 2-4My. The Dabbahu segment is also similar both in length and process to Quaternary rift segments in Afar. The high heat flux and broad, low form of the Erta 'Ale segment led Oppenheimer et al (2004) to propose that it comprises new igneous crust accreted by dyke intrusions, a process similar to that proposed for the subaerially exposed Asal spreading centre (Cattin et al., 2005).

As yet, no lavas have been observed along active faults, but field observations show small volume fissural flows along faults in Dabbahu segment are commonplace (Fig. SM3). Sanidine

feldspar lathes in pumice erupted from the Da'Ure vent, between Dabbahu and Gabho volcanoes, show resorption, indicating that their growth was interrupted by heating prior to eruption, consistent with a basaltic dyke intrusion model

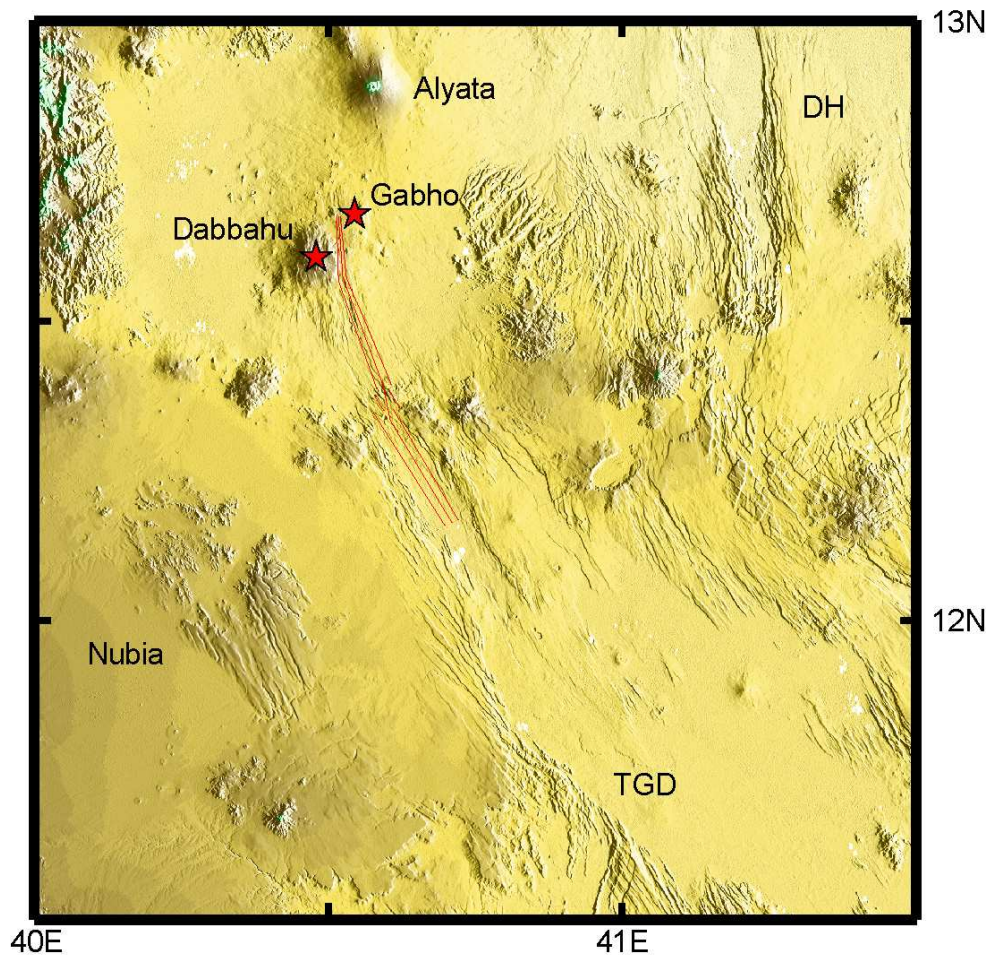


Figure SM1. SRTM 90 m DEM illustrates the morphology of the Dabbahu tectono-magmatic segment, and the distribution of Quaternary eruptive centres. Gabho and Dabbahu (red stars) are the two Quaternary centres that show subsidence in the InSAR data, indicating magma chamber depletion. Red lines are the positions of dykes in the simple elastic models. Note the dissected stratovolcanoes forming a chain perpendicular to the trend of the Dabbahu segment near its centres. TGD is the Tendaho-Goba'ad Discontinuity here separating the Nubia plate and the Danakil microplate. DH is Danakil horst, or, the Danakil microplate.

Field Photos of the Dabbahu magmatic segment

The Dabbahu tectono-magmatic segment lies in the plate boundary zone between stable Africa (Nubia) and the Danakil microplate to the northeast (Fig. SM1). Figures SM2 – SM5 illustrate characteristic features of the Dabbahu tectono-magmatic segment, as observed from several helicopter flights along and perpendicular to its length. Volcanological and structural observations from the four helicopter-assisted pre- and post-eruption visits to the Dabbahu site, as well as interviews of local pastoralists are provided in Yirgu et al. (2005) and Rowland et al. (2006).



Figure SM2. Photo of the Da'Ure eruptive centre, between Dabbahu and Gabho volcanoes, showing 170-175° striking fissures that cut ash units erupted on 26 September. South is to the top of the image.



Figure SM3. Photo of 170°-striking faults with fissural flows near the northern tip of the Dabbahu magmatic segment. Faults with extrusive lavas are common along the length of the Dabbahu segment. We do not believe any of these features were created in the 2005 event.



Figure SM4. Photograph (looking ~north) of a fault, marked by the arrows, that slipped 0.5 m down to the west during the September 2005 earthquake sequence.



Figure SM5. Photograph (looking ~north-east) of a fault near the centre of the Dabbahu rift segment that slipped by ~3 m (down to the west) during the rifting episode. Courtesy Julie Rowland, University of Auckland.

Seismological Methods

First arrival times recorded at International Monitoring System stations were used to relocate 100 of the 162 events in the International Seismological Centre (ISC) catalogue (Table SM1) – those that were recorded by 10 or more stations. Holding the location of the largest event (20050924, $M_w = 5.6$) fixed, and the depths fixed at 10 km, the epicentres were relocated using the Joint Epicentre Determination (JED) method of Douglas (1967). These estimates provide an average relative location error, within 90% confidence limits, of ± 8 km. The absolute location error of the fixed earthquake is 4-5 km.

The total seismic moment is estimated from the NEIC catalogue data using an empirical relation between body wave magnitude, m_b , and seismic moment, M_0 , for the central Afar region (Hofstetter and Beyth, 2003).

Date of Earthquake Yymmdd	Time of Earthquake hhmmss.ss	Lat	Long
050604a	184034.2	12.5732	40.635
050718a	163142.4	12.7823	40.7734
050914a	150746.9	12.5998	40.4335
050920a	21802.15	12.7585	40.4873
050920c	212338.2	12.7851	40.49
050920d	232707.2	12.7909	40.3949
050921a	143.44	12.8567	40.533
050921b	42122.22	12.714	40.549
050921c	71258.45	12.442	40.4977
050921d	84005.23	12.8719	40.5396
050921h	115724.2	12.6422	40.577
050921i	133301.8	12.5673	40.5369
050921j	145727.2	12.5921	40.5588
050921l	184402.9	12.6832	40.4602
050921m	200452.7	12.6088	40.6053
050921p	233630.2	13.1568	40.6424
050921q	234910.8	12.6207	40.5372
050922a	13132.97	12.8283	40.621
050922b	13937.34	12.6421	40.5305
050922d	31234.3	12.7085	40.5521
050922f	42818.89	12.7436	40.5845
050922i	101424.6	12.7443	40.4399
050922j	115744.1	12.7328	40.5027
050922l	135845.3	12.765	40.4644
050922o	195152.8	12.4475	40.557
050922p	222250.5	12.623	40.4673
050923b	45752.11	12.5984	40.5583
050923c	70609.55	12.622	40.5166
050923d	91832.09	12.659	40.5234
050923f	180126.6	12.7344	40.5452
050923h	202633.6	12.6452	40.5545
050924d	32526.13	12.8018	40.5022
050924e	33822.86	12.6445	40.5595
050924g	35715.23	12.6226	40.4742
050924i	41153.99	12.6882	40.525
050924j	42034.96	12.6903	40.4932
050924l	51534.48	12.6779	40.4684
050924m	53611.83	12.5041	40.447
050924n	54603.68	12.5826	40.3764
050924p	61045.29	12.6253	40.3911
050924q	61447.53	12.595	40.4669
050924r	62804.28	12.7058	40.4641

050924s	63247.01	12.729	40.6045
050924v	65828.61	12.7282	40.5871
050924x	73609.11	12.7004	40.5349
050924z	82049.38	12.5981	40.4714
050924aa	84137.38	12.6913	40.5648
050924bb	85222.1	12.8063	40.5266
050924cc	91715.6	12.61	40.4971
050924dd	95344.82	12.5634	40.4152
050924ee	163529.3	12.6064	40.4989
050924ff	180850.3	12.6224	40.5387
050924gg	192402.7	12.47	40.63
050924ii	221522.2	12.4004	40.5631
050924kk	223150.4	12.5349	40.622
050924mm	230520.8	12.4453	40.708
050924nn	232249.6	12.5103	40.6557
050925a	3729.06	12.5396	40.6745
050925c	11058.03	12.2364	40.4721
050925d	11129.84	12.2741	40.5414
050925e	11228.24	12.4849	40.4794
050925g	13146.21	12.4507	40.6555
050925j	35120.21	12.4321	40.5137
050925l	42644.92	12.4247	40.6349
050925m	51150.72	12.3845	40.5575
050925r	64736.84	12.3538	40.57
050925s	73928.48	12.3464	40.5854
050925t	81842.88	12.4637	40.6611
050925u	82130.95	12.3994	40.5978
050925w	83340.62	12.3495	40.5836
050925x	84450.86	12.6219	40.4639
050925cc	91137.7	12.4207	40.5924
050925ff	100212.8	12.3681	40.5593
050925gg	100757.7	12.4085	40.5977
050925hh	101800.9	12.5563	40.5274
050925kk	112004	12.4521	40.6562
050925mm	150914.7	12.4909	40.6288
050925nn	162203	12.4821	40.6822
050925qq	194756.4	12.3393	40.5764
050925ss	225404.9	12.4422	40.5446
050926a	25833.09	12.663	40.5413
050926b	93108.8	12.4453	40.5807
050926c	93354.12	12.4395	40.6283
050926d	132835.4	12.6428	40.5318
050926e	153626.5	12.6118	40.511
050926g	203002	12.474	40.609
050926h	212502.2	12.3933	40.6475
050926i	235311.6	12.545	40.4636
050927c	101358.5	12.6093	40.5726
050927e	161909.4	12.4521	40.6455
050927f	200826.8	12.4603	40.6061
050927g	202138.8	12.4435	40.661
050928a	2123.64	12.5187	40.4536
050928b	33610.88	12.6273	40.5214

050928d	161717.2	12.3776	40.5139
050928e	163136.1	12.458	40.6928
050929a	115220.2	12.471	40.6535
051001a	41621.66	12.6355	40.6669
051002a	232444.8	12.4029	40.6849
051004a	41940.97	12.4762	40.6542

Table SM3: Time and location of relocated earthquakes for the Dabbahu rifting episode. Depths are fixed at 10 km.

Radar Interferometry Methods

Interferograms and offset maps were constructed using ASAR images from ESA's ENVISAT satellite (Table SM2) and processed using JPL/Caltech ROI PAC software (Rosen et al., 2004). The topographic phase was removed using a 3 arcsecond 90 m resolution digital elevation model (DEM) generated by the NASA Shuttle Radar Topography Mission (SRTM) (Farr & Kobrick, 2000) and a power spectrum filter was applied (Goldstein & Werner, 1998). The interferograms were processed at full resolution to reduce incoherence caused by high phase gradients and unwrapped using a branch cut algorithm. Images showing the full resolution co-rifting interferograms are provided as supplementary data, along with kml files, for viewing in Google Earth TM.

Pre-rift interferograms are shown in figure SM6.

	Date 1	Date 2	Track	Timespan	Baseline
Co-rift	06-MAY-2005	28-OCT-2005	Descending (49)	5 months	250 m
Co-rift	28-JUL-2004	26-OCT-2005	Ascending (28)	15 months	390 m
Pre-rift	28-NOV-2003	16-APR-2004	Descending (49)	5 months	500 m
Pre-rift	16-APR-2004	06-MAY-2005	Descending (49)	13 months	270 m

Table SM2: Data from ESA's ENVISAT used to construct interferograms and offset maps.

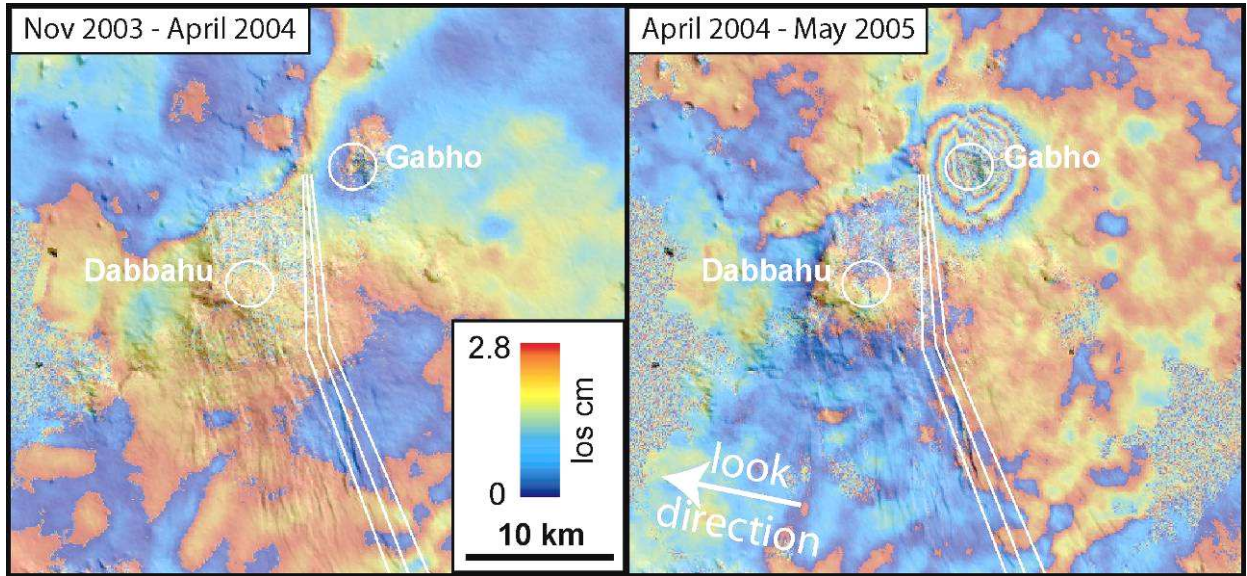


Figure SM6: Interferograms covering the Dabbahu region before the rifting event. a) No inflation is seen prior to April 2004 at either Gabho or Dabbahu volcanoes. b) Gabho volcano inflated by ~ 12 cm in the period April 2004 – May 2005 but no deformation is seen at Dabbahu volcano in the same time interval.

For the co-rift data (Fig 2), we estimate the east-west, north-south and vertical components of deformation at all pixels with, at minimum, descending range offset, ascending range offset and descending azimuth offset taking into account the variation of satellite line of sight across the scene (Wright et al., 2004). Unusually noisy or incoherent areas are masked out before inversion. The observations are weighted according to the noise estimated in the farfield (Table SM3). For each component, pixels with errors greater than 30 cm are masked out.

Observation	1-sigma uncertainty in line of sight (cm)
Descending Interferogram	0.6
Ascending Interferogram	1
Descending Range Offset	17
Ascending Range Offset	32
Descending Azimuth Offset	16
Ascending Azimuth Offset	11

Table SM3. Noise estimates for interferograms and offset maps.

References

- Barberi, F. & J. Varet, Volcanism of Afar: Small-scale plate tectonic implications, *Geol. Soc. Amer. Bull.*, **88**, 1251-1266 (1977).
- Cattin, R., C. Doubre, J.-B. de Chabaliere, G. King, C. Vigny, J.-P. Avouac & J.-C. Ruegg, Numerical modelling of quaternary deformation and post-seismic displacement in the Asal-Ghoubbet rift (Djibouti, Africa), *Earth Planet. Sci. Lett.* (2005).
- Douglas, A., Joint epicentre determination, *Nature*, **215**, 47-48 (1967).
- Farr, T., & Koblrick, M. Shuttle Radar Topography Mission produces a wealth of data. *Eos Trans. AGU*, **81**, 583-585 (2000).
- Goldstein, R. M., & Werner, C. L. Radar Interferometry filtering for geophysical applications. *Geophys. Res. Lett.*, **25(21)**, 4035-4038 (1998).
- Hayward, N., & C. Ebinger, Variations in the along-axis segmentation of the Afar rift system, *Tectonics*, **15**, **2**, 244-257 (1996).
- Hofstetter, R., & M. Beyth, The Afar Depression: interpretation of the 1960-2000 earthquakes, *Geophys. J. Int.*, **155**, 715-732 (2003).
- International Seismological Centre, *On-line Bulletin*, <http://www.isc.ac.uk/Bull>, Internatl. Seis. Cent., Thatcham, United Kingdom (2001).
- Oppenheimer, C., A. McGonigle, P. Allard, M. Wooster, V. Tsanev, Sulfur, heat, and magma budget of Erta Ale lava lake, Ethiopia, *Geology*, **32**, 509-512 (2004)
- Rowland, J.R., E. Baker & T. Kidande, Faults, fissures and other hazards associated with the Dabbahu rift event, Afar, 2005, Structural Field Report (*Pers comm*, 2006)
- Rosen, P. A., Hensley, S., Peltzer, G., & Simons, M. Updated Repeat Orbit Interferometry package released. *Eos Trans. AGU*, **85**, 35, (2004)
- Wright, T.J., Parsons, B.E., & Lu, Z. Towards mapping surface deformation in three dimensions using InSAR, *Geophys. Res. Lett.* **31(1)** L01607 doi:10.1029/2003GL018827 (2004)

Yirgu, G., D. Ayalew, A. Asrat, A. Ayele, and A. Philpotts,
<http://www.volcano.si.edu/reports/bulletin> (2005)